92 JS(2)

PREPARED FOR THE U.S. DEPARTMENT OF ENERGY,
UNDER CONTRACT DE-AC02-76-CHO-3073

PPPL-2825
JC-427

PPPL-2825

A PREDICTIVE TRANSPORT MODELING CODE FOR ICRF-HEATED TOKAMAKS

BY

C.K. PHILLIPS, W. HOULBERG, D.Q. HWANG,
S. ATTENBERGER, J. TOLLIVER, AND L. HIVELY

February 1992

PPPL PRINCETON PLASMA PHYSICS LABORATORY

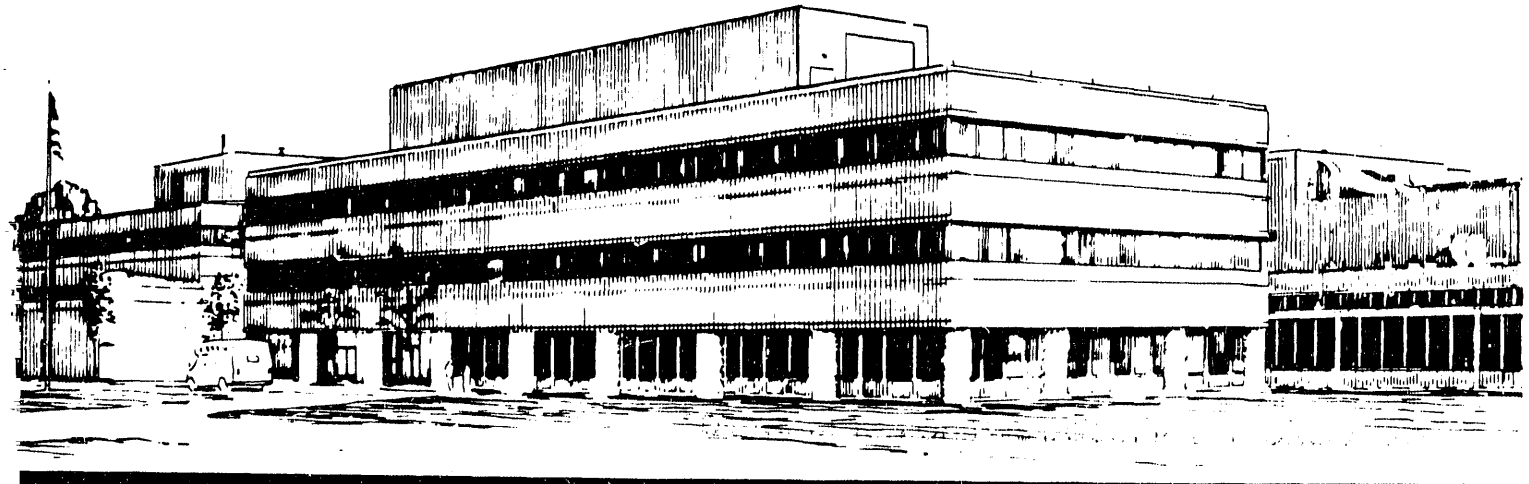

PRINCETON UNIVERSITY, PRINCETON, NEW JERSEY

NOTICE

This report was prepared as an account of work sponsored by an agency of the United States Government. Neither the United States Government nor any agency thereof, nor any of their employees, makes any warranty, express or implied, or assumes any legal liability or responsibility for the accuracy, completeness, or usefulness of any information, apparatus, product, or process disclosed, or represents that its use would not infringe privately owned rights. Reference herein to any specific commercial produce, process, or service by trade name, trademark, manufacturer, or otherwise, does not necessarily constitute or imply its endorsement, recommendation, or favoring by the United States Government or any agency thereof. The views and opinions of authors expressed herein do not necessarily state or reflect those of the United States Government or any agency thereof.

NOTICE

This report has been reproduced directly from the best available copy.

Available to DOE and DOE contractors from the:

Office of Scientific and Technical Information
P.O. Box 62
Oak Ridge, TN 37831;
Prices available from (615) 576-8401.

Available to the public from the:

National Technical Information Service
U.S. Department of Commerce
5285 Port Royal Road
Springfield, Virginia 22161
703-487-4650

PPPL--2825

DE92 008651

A PREDICTIVE TRANSPORT MODELING CODE FOR ICRF-HEATED TOKAMAKS

C.K. PHILLIPS, W. HOULBERG*, D.Q. HWANG#, S. ATTENBERGER*, J. TOLLIVER*, L. HIVELY*

Princeton Plasma Physics Laboratory, Princeton, NJ 08543

1. INTRODUCTION

Time-dependent transport simulations of tokamak discharges have been used extensively in recent years to gain an understanding of the plasma behavior in ongoing tokamak experiments as well as for extrapolating results to aid in design studies of proposed devices such as BPX (Burning Plasma Experiment) (formerly CIT, or Compact Ignition Tokamak) (PARKER *et al.*,1989; SIGMAR *et al.*, 1990; GOLDSTON, BATEMAN *et al.*, 1991; GOLDSTON, NEILSON *et al.*, 1991). One of the most important tasks which can be undertaken with these codes is the projection of the plasma operating conditions which can be achieved either in a new regime on an existing device or else in a new device which is being designed to meet a particular set of goals. Another important issue which can be addressed with these codes concerns the deduction and understanding of the transport properties of an auxilliary-heated tokamak. The basic idea is that the transport properties of the ions and electrons can be inferred from solutions of the particle and energy balance equations, provided that adequate models of the various source and sink terms in the equations can be constructed. In particular, in the case of tokamak plasmas heated with ICRF heating (Ion Cyclotron Resonance Frequency), an RF-heating module must be included in the transport simulation codes which can provide power deposition profiles to both the ions and the electrons as a function of time. The confidence which can be assigned to the deduced transport coefficients is directly dependent on the accuracy with which the source and sink terms can be represented.

*Oak Ridge National Laboratory, Oak Ridge, TN
#current address: University of California-Davis/Livermore, Dept. of Applied Science, Livermore, CA 94550

MASTER

To this end, an integrated time-dependent predictive transport/heating simulation package has been constructed which consists of the WHIST 2-D MHD equilibrium/1-D flux-surface-averaged transport code, developed by ORNL (HOULBERG, ATTENBERGER, and LAO, 1982), combined with the RAZE hybrid ray tracing/Fokker-Planck ICRF modeling code, developed by PPPL. The package is modeled after the BALDUR/ARF code package, developed originally by Hwang and Karney (1983) for modeling ICRF heating experiments in tokamaks with circular cross sections. The WHIST/RAZE package features the full capabilities of the WHIST code, including general 2-D axisymmetric equilibria and routines which model internal disruptions, pellet injection, neutral beam injection, gas puffing, impurity transport, radiation losses, fusion products, etc. The code can be used to study magnetic field and/or current ramp phases of a discharge, both of which may be important in the modeling of a device such as BPX. The RAZE code combines a ray tracing analysis of the ICRF wave propagation with a quasilinear analysis of the wave damping. A time-dependent isotropic Fokker-Planck module is incorporated, so that the evolution of the RF-induced fast ions can be followed. A ray tracing approach was chosen primarily due to time constraints which preclude the use of currently available full field methods. However, as a result, the simulation package is most suited to studying plasmas in which mode conversion is relatively weak and absorption is relatively strong.

In addition to the original BALDUR/ARF package, various alternate approaches to constructing a combined transport/heating package have been adopted by others. Most of the other predictive packages input ICRF power deposition profiles which are based on the results of stand-alone ICRF heating codes. For example, RF power deposition profiles calculated with the BRAYCO ray tracing code are used in combination with a bounce-averaged Fokker-Planck code BAFIC to determine RF power transfer profiles to the background thermal electrons and ions, which are in turn used as source functions in the JETTO $1^1/_2$-D transport code (BHATNAGAR *et al.*, 1990). Morishita, Fukuyama, and Furutani (1988) have constructed a time-dependent simulation package in which the ICRF power deposition profiles in 2-D equilibria are extrapolated from a 1-D kinetic model, based on geometric considerations, with collisional thermalization effects included with a modified moments solution to the Fokker-Planck equation. A similar model, in which 2-D power deposition profiles are constructed by projecting results from a 1-D kinetic analysis, has been incorporated by S.C.

Chiu (1989) in the ONE-TWO code of General Atomic (PFEIFFER *et al.*, 1980). Complementary transport "analysis" packages have also been developed recently. In particular, the TRANSP (HAWRYLUK, 1979) code uses SPRUCE (SMITHE *et al.*, 1987), a reduced order full field RF field code, coupled with FPP, a bounce-averaged Fokker-Planck solver (HAMMETT, 1986,1989).

In this report, a detailed description of the physics included in the WHIST/RAZE package as well as a few illustrative examples of the capabilities of the package will be presented. Some initial results from the package have been presented elsewhere (SWANSON *et al.*, 1987; HOULBERG *et al.*,1988). An in depth analysis of ICRF heating experiments using WHIST/RAZE will be discussed in a forthcoming report. A general overview of philosophy behind the structure of the WHIST/RAZE package, a summary of the features of the WHIST code, and a description of the interface to the RAZE subroutines are presented in section 2 of this report. Details of the physics contained in the RAZE code are examined in section 3. Sample results from the package follow in section 4, with concluding remarks and a discussion of possible improvements to the package discussed in section 5.

2. OVERVIEW OF THE WHIST/RAZE TRANSPORT SIMULATION PACKAGE

Integration of the WHIST transport simulation code with the RAZE ICRF modeling code is based on the premise that an ICRF-heated discharge is characterized by three distinct time scales: τ_E, the transport time scale, τ_C, the collisional thermalization time scale, and τ_W, the wave propagation and damping time scale. The plasma densities, temperatures, current and magnetic field profiles evolve on the longest time scale, τ_E. Typical values for τ_E range from 20 msec in mid-size tokamaks such as PLT (MAZZUCATO *et al.*,1985) to a couple of seconds in large devices such as JET (TUBBING *et al.*, 1989). The ICRF wave propagation and damping occur on the shortest time scale, τ_W, which is proportional to the time required for the waves to propagate from the antenna to the resonance layer. It scales as $a/(\omega/k_{perp}) \sim a/V_A$, where a is the plasma minor radius, ω is the wave angular frequency, k_{perp} is the perpendicular wave number, and V_A is the Alfven speed. Typical values range from $5*10^{-8}$ to 10^{-7} sec,

so processes which happen on the τ_W time scale are treated as instantaneous as far as the transport time scale is concerned. The ICRF-driven fast ion tail is formed and collisionally thermalizes with the background plasma on a time scale, τ_C, which is intermediate between τ_W and τ_E. It is typically significantly longer than τ_W, but may range in value from 50 msec to 300 msec or more, so it may be comparable to the transport time scale.

Evolution of the bulk plasma on the transport time scale is simulated by the WHIST transport code. The 1-D flux-surface-averaged time-dependent fluid transport equations are solved for the particle and energy flow as well as for the current diffusion in the tokamak. Time-dependent toroidal magnetic field ramps as well as plasma current ramps may be treated, either independently or simultaneously by the code. At any given time step, the 2-D MHD magnetic equilibrium is obtained from the Grad-Shafranov equation using the variational moments method (LAO, HIRSHMAN and WEILAND, 1981), assuming a fixed boundary condition.

The MHD equilibrium consists of simply nested flux surfaces, with no explicit separatrices. Flux surfaces are described with the coordinates (ρ,θ), where $\rho = \rho(\Phi)$ is a flux surface label, θ is a poloidal angle that increases by 2π the short way around the torus, and Φ is the toroidal magnetic flux enclosed between the flux surface $\rho(\Phi)$ and the axis of symmetry. However, in order to avoid singularities at the magnetic axis that occur in flux-based coordinate systems, Cartesian coordinates (R,Z) are used in the ray tracing algorithm in RAZE, where R is measured radially outwards from the major axis of symmetry of the tokamak, and Z is measured perpendicularly from the midplane. The cylindrical (R,ϕ,Z) components of the magnetic field and its derivatives, as well as the plasma densities and temperatures required by the ray tracing routines, are obtained in the following manner from the MHD equilibrium solution. In an axisymmetric system with up-down symmetry, the flux surfaces are represented by the expansion:

$$R(\rho,\theta) = \sum_{m=0}^{M} \rho^{m} \tilde{R}_m(\rho) \cos(m\theta)$$

$$Z(\rho,\theta) = \sum_{m=0}^{M} \rho^{m} \tilde{Z}_m(\rho) \sin(m\theta) \qquad (1)$$

with the amplitudes $\tilde{R}_m(\rho)$ and $\tilde{Z}_m(\rho)$ fitted by cubic splines to the solution at a discrete set of surfaces and the series truncated at M=2 in the VMOMS code (LAO, HIRSHMAN, and WEILAND, 1981). The flux surface coordinates (ρ_*,θ_*) of a specified point in cylindrical coordinates (R_*,Z_*) are determined by inversion of the above representation (ATTENBERGER, HOULBERG and HIRSHMAN, 1987). Plasma densities and temperatures, assumed constant on a flux surface, are interpolated from a cubic spline fit in ρ for values at ρ_*.

The cylindrical components of the magnetic field are obtained from the covariant field components as :

$$B_R = R_\theta B^\theta$$
$$B_\phi = R B^\zeta$$
$$B_Z = Z_\theta B^\theta \qquad (2)$$

where the subscripts on R and Z represent spatial derivatives of the cylindrical coordinates of a surface with respect to the flux surface variables. The covariant field components are:

$$B^\theta = \frac{\Phi'(\rho)}{2\pi R\tau q(\rho)}$$

$$B^\zeta = \frac{\Phi'(\rho)}{2\pi R\tau} \lambda_\theta(\rho,\theta) \qquad (3)$$

where $\tau = R_{,\theta} Z_{,\rho} - R_{,\rho} Z_{,\theta}$, $q(\rho)$ is the safety factor, $\Phi'(\rho)$ is the derivative of the toroidal flux with respect to the flux surface label, ρ, and λ is a stream function. The dimensionless radial coordinate, ρ, is defined in terms of the toroidal flux as $\rho \equiv \sqrt{\Phi(\rho)/\Phi_a}$ so that $\Phi'(\rho) = 2\rho\Phi_\alpha$, where Φ_a is the total toroidal flux enclosed by the plasma. The stream function is represented as an expansion of the form (HIRSHMAN and WHITSON, 1983):

$$\lambda(\rho,\theta) = \sum_{m=1}^{M_\theta} \rho^m \tilde{\lambda}_m(\rho) \cos(m\theta) \tag{4}$$

where the series is truncated at $M_\theta = 7$ and $\tilde{\lambda}_m(\rho)$ is fitted with a cubic spline to the solution on a discrete set of surfaces.

The derivatives of the cylindrical components of B are determined from finite differences, e.g.,

$$\frac{\partial B}{\partial R} \cong \frac{B_R(R + \delta R/2) - B_R(R - \delta R/2)}{\delta R} \tag{5}$$

with $\delta R \approx 5 \times 10^{-5}$ a. Use of the stream function representation for the magnetic field has forced the use of very small steps for the rays in order to maintain sufficient accuracy. This is most likely due to the fact that the field derivatives now involve second derivatives of the stream function. Earlier versions of the interface didn't have this difficulty when the covariant components were evaluated from:

$$B^\theta = \frac{\mu_0 I(\rho)}{2\pi R\tau \left\langle \frac{R_\theta^2 + Z_\theta^2}{R\tau} \right\rangle_\theta}$$

$$B^\zeta = \frac{\mu_0 F(\rho)}{2\pi R^2} \tag{6}$$

where $\langle A \rangle_\theta$ is the θ-average of A, $I(\rho)$ is the toroidal current enclosed within the surface, ρ, and $F(\rho)$ is the poloidal current external to the surface, ρ.

Regarding the use of specific transport models, the code is very flexible in that any given model can be easily incorporated by modifying the internal statements in one subroutine. Satellite modules are included which model phenomena which cause changes in the plasma on the shorter time scale. These modules (HOULBERG, ATTENBERGER, and LAO, 1982) can simulate internal disruptions, pellet injection, neutral beam heating, gas puffing, impurity transport, radiation processes, and, as discussed in this report, ICRF heating.

The RAZE code models the ICRF power deposition in the plasma. At any given time step in the transport simulation, it models the instantaneous net power deposition profiles which are contained in the auxiliary heating source terms in the transport equations. The power deposition profiles are recomputed in time as the plasma evolves, using instantaneous magnetic field geometry and plasma density and temperature profiles, which are provided by the WHIST code. The resonant ion distribution function is advanced in time with each call of the RAZE code. However, since the resonant ion distribution function can evolve on the intermediate time scale, τ_C, the distribution function is remembered from one transport time step to the next, so that corresponding changes in the ICRF power deposition that occur on the collisional time scale can be included. The connection between the resonant ion distribution function and the power deposition profiles is discussed in detail in the next section.

3. THE ICRF POWER DEPOSITION MODEL

ICRF power deposition profiles are constructed in the RAZE code by combining ray tracing to describe the ICRF wave propagation , quasilinear theory to calculate the wave damping, and an isotropic Fokker-Planck module to determine the effect of the waves on the resonant ion distribution function. The code is an extension of the Hwang and Karney ICRF modeling code (1983), with the main difference being that RAZE has been generalized to treat ICRF power deposition in a 2-D axisymmetric tokamak equilibrium with simply nested flux surfaces.

Wave propagation is described by ray tracing (BERNSTEIN, 1975) of the launched waves, using a warm, multi-fluid description of the plasma . Because the equilibrium is axisymmetric, only a 2-D ray tracing algorithm in a poloidal cross section of the tokamak is needed to construct 1-D flux-surface-averaged power deposition profiles. Plasma density, n_s, and temperature, T_s, profiles for each species, s, are assumed to be functions only of the flux surface,ρ. In Cartesian coordinates (R,Z), the ray tracing equations take the form:

$$\frac{dR}{dt} = -\frac{\partial D/\partial k_R}{\partial D/\partial \omega} \qquad \frac{dZ}{dt} = -\frac{\partial D/\partial k_Z}{\partial D/\partial \omega}$$

$$\frac{dk_R}{dt} = \frac{\partial D/\partial R}{\partial D/\partial \omega} \qquad \frac{dk_Z}{dt} = \frac{\partial D/\partial Z}{\partial D/\partial \omega} \tag{7}$$

where $D(k_\perp, k_{//}, n_s(\rho), T_s(\rho))$ is the dispersion relation for a warm, multi-fluid plasma, k_R and k_Z are the Cartesian components and $k_{//}$ and $k_\perp$ are the components of the wave vector parallel and perpendicular to the local equilibrium magnetic field,$\vec{B}$, and t denotes time along the ray path.

In the RAZE code, the evaluation of the derivatives in equation (7) have been formulated for a general 2-D simply-nested flux surface equilibrium by using local values of the magnetic field and its gradients. At any point along the ray path, the components of the equilibrium magnetic field and the Cartesian derivatives of these components, as well as the projections of the flux coordinate unit vectors onto the Cartesian coordinates and the derivatives of these projections are supplied by the WHIST code. For example, the term $\partial D/\partial R$ is evaluated using the chain rule for derivatives:

$$\frac{\partial D}{\partial R} = \frac{\partial D}{\partial \rho}\frac{\partial \rho}{\partial R} + \frac{\partial D}{\partial k_\perp}\frac{\partial k_\perp}{\partial R} + \frac{\partial D}{\partial k_{//}}\frac{\partial k_{//}}{\partial R} \quad , \tag{8}$$

where $\partial\rho/\partial R = -Z_\theta/\tau$, $\partial\rho/\partial Z = R_\theta/\tau$, with τ, R_θ, and Z_θ defined as in equations (2) and (3). Derivatives of the dispersion relation, D, with respect to ρ, $k_{//}$ and $k_\perp$ are easily evaluated since D is explicitly expressed in terms of these quantities. The derivatives of $k_{//}$ and $k_\perp$ with respect to R are constructed by applying the chain rule again. For example, $\partial k_{//}/\partial R$ can be expressed in terms of quantities supplied by WHIST by noting that

$$k^2 = k_\perp^2 + k_{//}^2 = k_R^2 + k_Z^2 + k_T^2$$

$$\text{where } k_T = \frac{\vec{k}\bullet\vec{B}_T}{B_T} = \frac{N_{tor}}{R} \tag{9}$$

and where N_{tor} is the toroidal mode number of the wave and B_T is the toroidal equilibrium magnetic field, and that

$$k_{//} = \frac{\vec{k}\bullet\vec{B}}{B} = \frac{k_T B_T + k_p B_p}{B}$$

$$\text{where } k_p = k_R \hat{R}\bullet\hat{\theta} + k_Z \hat{Z}\bullet\hat{\theta} \tag{10}$$

where $\hat{\theta}$ is the unit vector in the poloidal direction along a flux surface, $\hat{R}$ and $\hat{Z}$ are the unit vectors in the Cartesian directions, and B_P is the poloidal component of the equilibrium magnetic field. By using equations (9)-(10), the term $\partial k_{//}/\partial R$ can now be constructed in the form:

$$\frac{\partial k_{//}}{\partial R} = \frac{-k_{//}}{B}\frac{\partial B}{\partial R} + \frac{1}{B}\left[k_T\frac{\partial B_T}{\partial R} + k_P\frac{\partial B_P}{\partial R} - \frac{k_T B_T}{R} + B_P\left(k_Z\frac{\partial c}{\partial R} - k_R\frac{\partial s}{\partial R}\right)\right] \tag{11}$$

where c and s are defined as

$$\hat{Z}\bullet\hat{\theta} \equiv c = \frac{\dfrac{\partial\rho}{\partial R}}{\sqrt{\left(\dfrac{\partial\rho}{\partial R}\right)^2 + \left(\dfrac{\partial\rho}{\partial Z}\right)^2}} \qquad \hat{R}\bullet\hat{\theta} \equiv -s = \frac{\dfrac{\partial\rho}{\partial Z}}{\sqrt{\left(\dfrac{\partial\rho}{\partial R}\right)^2 + \left(\dfrac{\partial\rho}{\partial Z}\right)^2}} \quad . \tag{12}$$

Note that $\partial k_{//}/\partial R$ involves derivatives of the terms c and s so that second derivatives of the flux function are needed. In a plasma with concentric, circular flux surfaces, the term s, for example, is readily evaluated as

$$s_{(circular)} = \frac{Z}{\sqrt{(R-R_0)^2 + Z^2}} \tag{13}$$

where R_0 is the major radius. However, in a general 3-D equilibrium (requiring the use of a stream function), accurate and efficient numerical evaluation of second order derivatives of the flux function is difficult to achieve over the same spatial distance needed when flux functions are used to expand the field components as discussed in Section 2 (ATTENBERGER, HOULBERG, and HIRSHMAN, 1987). Numerical jitter in these terms leads to an increase in the number of step-size halvings in the predictor-corrector routines which are used to integrate the ray equations in phase space. As a result, approximately 30-50% more steps are required in tracing a ray over the same spatial distance in the general 2-D numerically-specified equilibrium as opposed to an analytically specified concentric, circular flux surface equilibrium. Similar considerations apply to the remaining terms in equations (7).

In a typical simulation of the wave fields, the ray paths for 20 rays are determined by numerical integration of equations (7). By increasing the number of rays included in the simulation, smoother power deposition profiles can be derived. However, the computational time required also increases. An arbitrary coupled wave spectrum can be handled by the code by specifying initial values for the starting positions ρ_i, θ_i , the toroidal and poloidal mode numbers $N_{tor,i}$, M_i and the powers P_i for each of the i rays included in the simulation. The spectral characteristics of the launched waves a e assigned on the basis of stand-alone coupling codes. A Newton's iteration is performed at each starting location for each ray to self-consistently determine the initial values of $k_\perp$ which satisfy the dispersion relation. A particular ray is followed until its power drops below a preset level, typically 10% of its starting power, or until it has been integrated through a preset number of steps, typically 400-600, which is generally sufficient to allow the ray to make at least three pass-

es between the launcher and the resonance layer. At the plasma edge, an approaching ray is specularly reflected, with a user-specified power loss, back into the plasma. This latter loss provides an option to heuristically mock-up losses which are not included in the ICRF model, such as fast ion losses or power losses to the plasma limiters, etc.

Wave damping is calculated from the ICRF-induced quasilinear diffusion of an isotropic distribution of resonant particles. As any given ray,i, travels through each radial zone, the flux-surface-averaged power, $p_{d,s,i}(\rho)$, that it deposits on each plasma species,s, is calculated using the quasilinear tensor, $\overleftrightarrow{D}_{QL,s,i}$,as defined by Kennel and Engelmann (1966), attributed to ray i:

$$p_{d,s,i}(\rho) = \text{power absorption/vol} = -\int d^3v \; n_s \; m_s \; \vec{v} \bullet \overleftrightarrow{D}_{QL,s,i} \bullet \frac{\partial f_s}{\partial \vec{v}} \tag{14}$$

where $f_s(\vec{r})$ is the isotropic distribution function for species s, m_s is the mass of a particle of species s, and the integration is over velocity,$\vec{v}$. Since the full quasilinear diffusion operator is evaluated from the wave electric fields, all resonant interactions between the wave fields and the particles, such as Landau and cyclotron harmonic absorption, are included in the damping calculation. Because WHIST solves flux-surface-averaged fluid transport equations, the power deposition profiles are calculated in RAZE assuming rapid equilibration of the wave damping along a flux surface. Around a given flux surface with flux surface area, $A(\rho)$, and differential volume, $\Delta V(\rho)$, a single ray with a local power equal to $P_i(\rho)$ contributes an amount $\Delta U_i(\rho)$ to the local flux-surface-averaged wave energy density, determined by

$$\frac{\Delta U_i}{\Delta t}(\rho) = \frac{P_i}{\Delta V}(\rho) = \frac{P_i(\rho)}{|v_{g\rho}| \Delta t \, A(\rho)} \Rightarrow \Delta U_i(\rho) = \frac{P_i(\rho)}{|v_{g\rho}| \; A(\rho)} \quad , \tag{15}$$

where the $\hat{\rho}$ component of the wave's group velocity is denoted by $v_{g\rho}$. The local energy density of the wave is related to the local wave electric fields through the dispersion tensor, $\overleftrightarrow{D}$, using the well-known relation (Stix, 1962)

$$\Delta U_i(\rho) = \frac{1}{4}\varepsilon_0 \omega \vec{E}^* \cdot \frac{\partial \overleftrightarrow{D}}{\partial \omega} \cdot \vec{E} = \frac{1}{4}\varepsilon_0 \omega E^2 \hat{e}^* \cdot \frac{\partial \overleftrightarrow{D}}{\partial \omega} \cdot \hat{e} \quad , \tag{16}$$

where the local electric field vector, $\vec{E}$, has been written in terms of its local magnitude, E, and polarization vector, $\hat{e}$, as

$$\vec{E} = E\,\hat{e}\exp[i(\vec{k}\cdot\vec{r} - \omega t)] \quad , \tag{17}$$

and where the polarization vector satisfies the relations:

$$\overleftrightarrow{D}\cdot\hat{e} = 0 \quad \text{and} \quad \hat{e}^*\cdot\hat{e} = 1 \quad . \tag{18}$$

The superscript * denotes the complex conjugate of the associated variable. Using equations (14)-(17), the contribution from ray i to the quasilinear diffusion tensor (KENNEL and ENGELMANN, 1966) can be evaluated locally in terms of the wave fields according to:

$$\begin{aligned}
\overleftrightarrow{D}_{QL,s,i} &= \frac{\pi}{2}\sum^{N}\frac{q_s^2}{m_s^2}\,\delta\left(\omega - k_{//}v_{//} - N\Omega_s\right)E^2\,\vec{a}_N^{\,*}\vec{a}_N \equiv \frac{P_i(\rho)}{|v_{g\rho}|A(\rho)}\overleftrightarrow{Q}_s \\
\vec{a}_N &= \theta_N\frac{k_{//}}{\omega}\left[\left(\frac{\omega}{k_{//}} - v_{//}\right)\hat{v}_\perp + v_\perp\hat{v}_{//}\right] \\
\theta_N &= \frac{e_r J_{N+1} + e_l J_{N-1}}{\sqrt{2}} + \frac{v_{//}}{v_\perp}J_N e_{//}
\end{aligned} \tag{19}$$

where N denotes the harmonic interaction number, Ω_s is the cyclotron angular frequency for species s, $\hat{v}_\perp$ and $\hat{v}_{//}$ are perpendicular and parallel unit vectors in velocity space, J_N is the Nth order Bessel function with

argument $\frac{k_\perp v_\perp}{\omega}$, and e_l, e_r, and $e_{//}$ are the left-hand, right-hand, and parallel components of the polarization vector defined in equations (17) and (18). In practice, only the $\perp\perp$ and the // // components of $\overleftrightarrow{D}_{QL,s,i}$ are used in the simulation code, since the minority distribution function is approximated to be isotropic in velocity space. By inserting equation (19) into equation (14), the local power absorption on species s can be written in terms of the local power in the ith ray as

$$p_{d,s,i}(\rho) = -\int d^3v \; n_s m_s \vec{v} \cdot \overleftrightarrow{D}_{QL,s,i} \cdot \frac{\partial f_s}{\partial \vec{v}} \equiv \frac{P_i(\rho)}{|v_{g\rho}| A(\rho)} C_s \quad . \tag{20}$$

Hence, as the ray propagates, it is damped according to

$$\frac{dP_i(\rho)}{dt} = -p_{d,i}(\rho) |v_{g\rho}| A(\rho) = -P_i(\rho) \; C$$

so

$$P_i(\rho) = P_{i0} \exp(-Ct) \tag{21}$$

where P_{i0} is the initial power in the ray, and C and $p_{d,i}$ denotes a sum over species of equation (20).

The wave damping, as determined from equation (21) by summing over contributions from all the rays, represents only direct damping of the waves by resonant interactions with the plasma. In most regimes of interest, the ICRF waves tend to damp preferentially on the resonant ion species, thereby driving the distribution function of the resonant species to be non-Maxwellian, characterized by a high energy tail (STIX, 1975). The hot ions in the tail collisionally interact with the background species, thereby redistributing the absorbed wave energy to the bulk plasma species. However, the wave energy absorbed by the minority species will be equal to the energy collisionally redistributed to the bulk species only under steady-state conditions. Otherwise, the difference between the wave energy input to the minority species and the collisional energy lost from the minority to the background ions causes the minority distribution function to evolve in velocity space. In any case, the net power deposition

from the waves to the bulk plasma species is a combination of direct wave damping plus indirect heating via collisional thermalization of the ICRF-induced fast ions. Note that the net heating of the bulk minority ions consists only of power which is collisionally transferred from the hot tail minority ions.

In order to model the collisional contributions to the net power deposition profiles, the distribution function, f_m, of the resonant, or minority, ion species is self-consistently evolved using a time-dependent, isotropic Fokker-Planck solver in each radial annulus of the plasma cross section. By choosing an isotropic model for the minority distribution function, effects which are directly related to the velocity-space anisotropies caused by high-power ICRF heating have been neglected. Bounce-averaged Fokker-Planck models for the fast ion distribution function have been developed recently (KERBEL and MCCOY, 1985; HAMMETT, 1986) which can address some of the issues associated with velocity-space anisotropies. However, the models tend to require significantly more computational time than the isotropic model assumed here. Though the use of these more complex models in a predictive transport simulation would undoubtably increase the accuracy of the predicted power deposition profiles, the associated increase in computational time would tend to render the simulation package impractical as far as day-to-day studies of experiments are concerned.

Both Coulomb collisions and ICRF-induced quasilinear diffusion are included in the model Fokker-Planck equation for f_m in each radial annulus:

$$\frac{\partial f_m}{\partial t} = \left(\frac{\delta f_m}{\delta t}\right)_{coll} + \frac{1}{v^2}\frac{\partial}{\partial v} v^2 \sum_{\substack{\text{ray} \\ \text{crossings}}} D_{QL,m} \frac{\partial f_m}{\partial v} \quad , \tag{22}$$

where $D_{QL,m}$ is the $\widetilde{vv}$ component of the quasilinear diffusion tensor, averaged over pitch angle and determined by summing over the contributions from each of the rays that crossed the given annulus. The resonant ion distribution function is initialized to be a local Maxwellian at the bulk ion temperature in each radial annulus and is then evolved in time using equation (22). The time step used to advance equation (22) is equal to the transport time that has elapsed since the rf subroutines were last called by WHIST. In evaluating the collisional terms in equation (22), the background species are all assumed to be Maxwellians at the bulk ion

temperature. This approximation is made so that the rf subroutines calculate the collisional transfer of energy from the hot tail ions to the bulk species while WHIST calculates temperature equilibration between the bulk ions and electrons. Collisional redistribution of the power absorbed by the minority species to the bulk species is determined from equation (22) and is added to the direct wave damping profiles, as determined using equation (21), to arrive at the net power deposition profiles to the background species. Net power deposition profiles to the bulk ions and electrons are then passed, through the interface routines, to WHIST for use in the energy balance equations.

In a typical simulation of an ICRF-heated discharge, WHIST first evolves the plasma through the pre-RF phase of the discharge. During the ICRF heating phase, the RAZE routines are called whenever the input power or the background plasma conditions have changed by a user-specified relative amount, typically chosen as 10%, or else if a user-specified transport time interval has passed. When sawteeth are present in the discharge, additional calls to the RAZE routines are made in order to include the effects of sawtooth mixing on the fast ion distribution function. After each occurrence of a sawtooth, the RAZE package is called and the fast ion distribution function is averaged over the mixing radius to reflect the effect of sawtooth mixing of the fast ions (PHILLIPS *et al.*,1989). An estimate of the fast ion slowing down time is then obtained and compared to an estimate of the sawtooth period, based on experimental observations or else sawtooth period scaling laws such as the one proposed by Park and Monticello (1990). If the slowing down time is less than the estimated sawtooth period, then the RAZE code is called up an additional four times over a time period equal to the estimated slowing down time and then at subsequent times as needed, as specified above. On the other hand, if the slowing down time is longer than the estimated sawtooth period, then the RAZE code is called an additional four times over a time interval equal to the estimated sawtooth period. Depending on the particular plasma conditions being simulated, which influence such factors as the strength of the wave absorption and the length of the velocity grids required to adequately represent the minority distribution function, one complete call of the RAZE package can take from one to five minutes of cpu time on a CRAY-XMP. It is therefore desirable to minimize the number of times that RAZE is called by WHIST, subject to the constraint that the time evolution of the power deposition profiles be realistically determined. In the next section, a few illustrative examples of the capabilities of the combined

WHIST/RAZE package will be discussed.

4. SAMPLE RESULTS

Predictive transport simulations of tokamak plasmas require the specification of a suitable model for the particle and energy transport. Though a great deal of progress has been made in recent years towards developing theory-based semi-empirical transport models which can be used to successfully simulate the behavior of plasmas in current experiments, a single model has yet to be found which can be used reliably under all conditions of interest (REDI and BATEMAN, 1991; REDI *et al.*, 1987). In order to illustrate the capabilities of the WHIST/RAŻE package in simulating ICRF heating experiments in tokamaks, a simple transport model has been formulated based on empirically derived global scaling relations and experimentally deduced radial profiles for the thermal conduction coefficients. Simulations of ICRF heating experiments on PLT and projections to the operating regime which may be attained on the proposed ignition device BPX (PARKER *et al.*,1989; SIGMAR *et al.*, 1990; GOLDSTON, BATEMAN *et al.*, 1991; GOLDSTON, NEILSON *et al.*, 1991), will be discussed in this section using this simplified model.

In tokamaks, the electron and ion thermal heat conduction coefficients, χ_e and χ_i, respectively, are generally assumed to consist of an anomalous contribution, χ^{anom}, plus the neoclassical term, χ^{neo}. The anomalous contribution tends to dominate the behavior of the plasma, leading to energy confinement times which are substantially lower than would be predicted on the basis of the neoclassical theory alone. A simple model for χ^{anom} can be constructed by assuming that the conduction coefficients can be written in the form:

$$\chi_e^{anom}(\rho) = \chi_{e0} f(\rho) \tag{23}$$

where χ_{e0} is a normalization factor and $f(\rho)$ describes the radial variation of the heat conduction across the plasma minor radius. The radial varia-

tion of χ_e^{anom} is specified based on the behavior deduced from analysis of experiments. A typical form that has been used in the simulations presented in this paper is :

$$f(\rho) = \frac{\left[1 + \left(2\frac{r_m}{a_m}\right)^4\right]}{2} \quad \text{for } \frac{r_m}{a_m} \geq 0.25$$

$$f(\rho) = \frac{1}{2}\frac{\left[1 + \left(2\frac{r_m}{a_m}\right)^4\right]}{2} \quad \text{for } \frac{r_m}{a_m} < 0.25 \tag{24}$$

where r_m and a_m denote the flux surface radius and the plasma minor radius evaluated on the midplane, respectively. The normalization factor, χ_{e0}, can be derived from the global scaling relations for the energy confinement time, as described below.

Global scaling relations for the energy confinement time, τ_{exp} , are generally derived from experimental data using the energy balance equation in the steady state limit:

$$\frac{dW_{tot}}{dt} = P_{in} - \frac{W_{tot}}{\tau_{exp}} = 0 \tag{25}$$

where W_{tot} is the total stored energy in the plasma and P_{in} denotes the total input power, including ohmic and auxiliary sources. By rewriting the energy balance equation in terms of conduction and other losses, the energy confinement time can be related to the electron and ion thermal diffusivities as follows:

$$\frac{dW_{tot}}{dt} = P_{in} - P_{cx} - P_{rad} - P_{ion} - \int d^3x \left(\nabla\cdot q_e + \nabla\cdot q_i\right) \quad , \tag{26}$$

where the integration is over the plasma volume. Losses due to charge exchange, radiation, and ionization are denoted by P_{cx}, P_{rad}, and P_{ion}, respectively, while the conduction and convection losses are contained in $\vec{q}_e$ and $\vec{q}_i$ as:

$$\vec{q}_j = \vec{q}_j^{\,cond} + \vec{q}_j^{\,conv} = - n_j \chi_j \frac{\partial T_j}{\partial \rho} \hat{\rho} + \vec{q}_j^{\,conv} \tag{27}$$

for j=i,e. The anomalous portion of χ_i is usually set to be proportional to the anomalous electron thermal diffusivity:

$$\chi_i(\rho) = \alpha \, \chi_e^{anom}(r) + \chi_i^{neo}(r) \tag{28}$$

where α denotes the proportionality constant. This assumption is consistent with both D-III-D and TFTR data, when α is set in the range of 0.5-5 (ZARNSTORFF *et al.*,1988).

Having specified the radial dependence of the thermal conduction coefficients, equations (25)-(26) may now be equated to determine the overall normalization of χ_e, consistent with the chosen global scaling law for τ_{exp}. The result may be written in the form:

$$\chi_{e0} = \frac{-1}{f(a_m)} \frac{\dfrac{W_{tot}}{\tau_{exp}} - P_{loss} + S\, n_i(a_m)\, \chi_i^{neo} \dfrac{\partial T_i(a_m)}{\partial \rho} + S\, n_e(a_m)\, \chi_e^{neo} \dfrac{\partial T_e(a_m)}{\partial \rho}}{S \left[\alpha\, n_i(a_m) \dfrac{\partial T_i(a_m)}{\partial \rho} + n_e(a_m) \dfrac{\partial T_e(a_m)}{\partial \rho} \right]} \tag{29}$$

where

$$P_{loss} = P_e^{conv} + P_i^{conv} + P_{cx} + P_{ion} + P_{rad} \tag{30}$$

and where S denotes the surface area of the outermost flux surface. To

insure that the simulation reproduces the desired global scaling for τ_{exp}, equation (29) for the normalization constant for the anomalous thermal diffusivity must be reevaluated at each time step, using the current values for densities, temperatures, etc. Estimates for the neoclassical contributions and for the loss terms can be saved from the previous timest p, if necessary, to complete the evaluation of χ_{e0}.

The WHIST/RAZE simulation package has been used to study the high power ICRF heating experiments performed on the PLT tokamak which were reported by Mazzucato et al. (1984) and Wilson et al. (1985). In these experiments, up to 5 MW of ICRF power at 30 Mhz was applied to the PLT plasma in the deuterium majority/helium-3 minority mode of heating. The power was applied on the low field side of the torus with three half-turn antennas, phased such that the launched spectrum was peaked around 10 m^{-1}. A striking feature observed for the first time in these experiments was the occurrence of giant sawtooth oscillations during the RF heating interval in which $\Delta Te/Te(0)$, where ΔTe is the change in the central electron temperature, $Te(0)$, due to a sawtooth oscillation, was on the order of 33% (MAZZUCATO *et al.* 1984; WILSON *et al.* 1985; CAVALLO *et al.* 1985). The observed energy confinement time was consistent with the Goldston Aachen L-Mode scaling relationship (GOLDSTON *et al.* 1984), except for some evidence that the decrease in confinement time with increasing ICRF power level saturated for powers above 3 MW (WILSON *et al.* 1985). Results of a comparison between the measured temporal evolution of the central electron and ion temperatures and simulations using the WHIST/RAZE package are shown in Fig.1 for 2.6 MW coupled to the plasma. The electron and ion density profiles in the simulation were adjusted to match the experimental profiles, as reported by Mazzucato et al. (1984). The electron and ion energy transport was simulated with the model specified above in equations (23),(24),(28),(29), and (30) with τ_{exp} replaced by the Goldston Aachen L-mode scaling relation (GOLDSTON, 1984),

$$\tau_G = \frac{5.8e\text{-}8\ \kappa^{0.5}\ I_P\ R_0^{1.75}}{P_{in}^{0.5}\ a_m^{0.37}} \tag{31}$$

where I_p is the plasma current in amps, κ is the plasma elongation measured at the plasma edge, R_0 and a_m are the plasma major and midplane minor radii measured in centimeters, and P_{in} is the total input power in watts. In the simulation, τ_G has been multiplied by 0.9 (in order to reproduce the experimentally observed value of 21 msec at the peak of the RF power pulse) and with α=0.4. Reasonable agreement is found between the experimental measurements and the simulation results, including reproducing the measured sawtooth amplitude on the central electron temperature. The sawtooth modulation of the ion temperature was not measured with the diagnostics used for the data given in Fig.1. However, measurements of the ion temperature with an x-ray crystal spectrometer indicate that the amplitude modulation of the central ion temperature due to sawtooth oscillations was comparable to that observed for the central electron temperature (BITTER *et al.* 1981). In these experiments, the sawtooth period was about 10 msec while the fast ion slowing down time was on the order of 50-100 msec. Since the slowing down time is of the same order as the time for the minority tail to be formed, an interesting consequence of the relatively rapid sawtooth period is that the minority tail temperature remained relatively low and the power deposition profiles were severely flattened over the q=1 volume. In Fig. 2, the calculated power deposition profiles to the ions and the electrons at the bottom of a sawtooth oscillation are displayed. The calculated central heating rate of electrons of approximately 1.5 W/cm^3 is in excellent agreement with the measured value, as reported by Mazzucato et al. (1984). To test the predictive capability of this simple transport model, the input power in the simulation was raised to 4.3 MW while all other inputs were left unchanged and the results were compared to the data taken in experiments on PLT conducted at that input power. As shown in Fig. 3, the use of even this simple transport model in the WHIST/RAZE package yields calculated temperatures which scale reasonably with the experimental observations.

The simple transport model described in this section has also been used to project the confinement performance and ICRF heating power deposition profiles which may be obtainable in an ignition tokamak such as the proposed BPX device. BPX is a high field (B_T ~ 8-9 T), relatively compact (R_0~2.59 m, a~0.8 m) tokamak with noncircular flux surfaces

(κ_{95}~2, δ_{95}~0.35) designed to study self-heated plasmas with Q>5 which produce significant fusion power yields using auxiliary heating based on 20 MW of ICRF or 50 MW of combined ICRF and ECRH (Electron Cyclotron Resonance Heating) (PARKER *et al.*,1989; SIGMAR *et al.*, 1990; GOLDSTON, BATEMAN *et al.*, 1991; GOLDSTON, NEILSON *et al.*, 1991). The machine is designed to run with central electron densities of about $3*10^{20}$ m^{-3}, with density profile shapes ranging from the very flat profiles seen in current devices in H-mode operation to moderately peaked profiles which can be obtained with pellet injection (GOLDSTON, R.J., NEILSON, H. *et al.*, 1991). For the sample cases discussed in this report, the profile is assumed to be moderately peaked, as depicted in Fig. 4. During the time that the ICRF heating is applied, the plasma current and toroidal magnetic field undergo very weak ramp phases prior to the start of flattop operation, as shown in Fig. 5. The confinement performance has been projected using the simple transport model described in this section, with the empirical scaling relation for the energy confinement time evaluated using either the more pessimistic ITER89-P L-Mode scaling (YUSHMANOV *et al.*, 1990),

$$\tau_{ITER89P} = \frac{3.81e\text{-}9\ \kappa^{0.5}\ \mu_{eff}^{0.5}\ I_P^{0.85}\ R_0^{1.2}\ a_m^{0.3}\ n_e^{0.1}\ B_T^{0.2}}{P_{in}^{0.5}} \tag{32}$$

where μ_{eff} is the average mass of the ion species, B_T is given in tesla, and n_e is given in m^{-3}, or else the more optimistic ITER-H H-Mode scaling (CHRISTIANSEN *et al.*, 1990):

$$\tau_{ITER\text{-}H} = \frac{2.59e\text{-}8\ \kappa^{-0.19}\ \mu_{eff}^{0.5}\ I_P^{1.02}\ R_0^{1.6}\ B_T^{0.15}}{P_{in}^{0.47}} \quad . \tag{33}$$

Fig. 6 displays the projected temperature evolution of a BPX plasma using these two scaling relations. It was assumed that $x_{i,anom}/x_{e,anom}=1$ in these examples, though other runs with the ratio varied from 0.5 to 2.0 gave very similar results. Since ray tracing codes tend to predict power deposition profiles which are more strongly peaked than full wave codes (BRAMBILLA and KRUCKEN, 1988; KRUCKEN and BRAMBILLA, 1989; TIBONE *et al.*, 1988; PHILLIPS *et al.*, 1989), the ICRF resonance layer was placed

somewhat off-axis on the high field in order to more realistically model the power deposition density in the central region of the discharge. A Kadomstev model for sawtooth oscillations was utilized, with the trigger for a sawtooth event determined by q(0) dropping below 1 on axis. In both cases, extreme modulation of the central electron and ion temperatures is projected due to sawtooth events. Though this effect is consistent with the observations of giant sawteeth on PLT (MAZZUCATO *et al.*, 1985), TFTR (PHILLIPS *et al.*, 1989; HOSEA *et al.*, 1990), and JET (GILL *et al.*, 1986), the exact extent to which the temperature amplitude will be modulated is dependent on a balance between the strong central peaking of the ICRF heating deposition profile, the associated suppression of χ_e and χ_i in the core, and on the size of the q=1 volume. The simple transport model used here includes a reduction of χ_e and χ_i for the inner quarter of the minor radius, as indicated in equation (24). This model is consistent with the PLT observations described above as well as with simulations of ICRF-heated, pellet-fueled discharges in JET (HOULBERG *et al.*, 1989). The sawtooth period is longer in the simulation using the more optimistic ITER-H scaling since the calculated central electron heating rate is significantly higher in that case. The ICRF heating power split between ions and electrons for the two cases is shown in Fig. 7. For both scenarios, ion heating is more dominant than electron heating, though in the simulation using ITER-H scaling, significantly more direct electron heating is predicted towards the end of the flattop phase due to the higher achieved electron temperature, so that the power split to ions and electrons becomes more even. Finally, based on the results of these simulations shown in Fig. 8, the projected fusion gain, Q, is ≥ 5 even if the best confinement achievable in BPX is limited by L-mode type confinement, as embodied in the ITER89-P scaling. Hence, it is likely that BPX has been adequately designed to study the physics of self-heated fusion plasmas, including the production of substantial amounts of fusion power (GOLDSTON, NEILSON *et al.*,1991; GOLDSTON, BATEMAN *et al.*, 1991).

5. SUMMARY AND CONCLUSIONS

A predictive transport/heating simulation package has been developed for studying ICRF-heated tokamak discharges by integrating the WHIST $1^1/_2$-D predictive transport code with the RAZE ICRF power deposition code. The package is capable of self-consistently recomputing the ICRF power deposition profiles and the resonant ion distribution function as a

function of time as the equilibrium plasma evolves on the transport time scales. Though the evolution of the tokamak discharge is affected most significantly by the transport properties of the plasma and by global phenomena such as sawtooth oscillations, significant changes in the split of applied ICRF power to the electrons and the ions can occur throughout the heating phase of the discharge, thereby influencing the overall plasma performance.

A number of approximations have been made which limit the applicability of the package. Two main assumptions pertain directly to the WHIST code. First of all, WHIST equilibria consist of simply-nested flux surfaces, so that simulations of ICRF heating in diverted configurations are valid only for regions within the separatrices. Secondly, the transport of the bulk species in the WHIST code is accomplished assuming that the bulk species are Maxwellian. Transport effects related to the ICRF-induced hot tail ions are neglected on the basis that the relative population of these particles is small and that initial measurements of the transport of these ions is small relative to the anomalous transport properties of the bulk species (HAWRYLUK, R. 1991). However, in plasmas in which second harmonic ICRF heating of a bulk ion species becomes significant, large fractions of the plasma can become very non-Maxwellian in character (HWANG *et al.*, 1983). In this case, different models for the conduction and convection losses would need to be developed and incorporated into the code.

The RAZE code uses ray tracing techniques to model the wave propagation and electric fields in a warm, multifluid plasma, and hence is subject to the usual weaknesses of WKB and "cold" plasma models. In particular, the approximations break down in the absorption region, so that solutions for the field polarizations are inaccurate and mode conversion and kinetic effects on the wave absorption are neglected. Furthermore, coherence effects, such as diffraction and cavity mode formation, are also neglected in ray tracing models. Despite these limitations, a ray tracing model was chosen because it is possible to estimate the damping due to a general launched spectrum of waves in a relatively minimal amount of time compared to full field methods which utilize kinetic models for the absorption. For example, one complete call of the RAZE code, as implemented in WHIST, requires from one to five minutes of CRAY cpu time to calculate the combined direct and collisional power deposition profiles due to 20 rays, each of which may have a different $k_{//}$, as well as evolve the minor-

ity distribution function. By comparison, 2-D stand-alone full field kinetic models (FUKUYAMA *et al.*,1986; BRAMBILLA and KRUCKEN,1988; EDERY *et al.*,1987) typically require five or more minutes of cpu time to determine the direct damping profiles for a single value of $k_{//}$. Full field codes (SMITHE *et al.*,1987; BATCHELOR *et al.*,1989) which utilize reduced order representations for the kinetic effects require less time, on the order of one cpu minute per $k_{//}$. These latter codes may be candidates for replacement of the ray tracing modules in the predictive code packages, though their use will entail an increase in overall run time. Another possible candidate is a hybrid ray tracing/mode conversion model (PHILLIPS,1985) in which ray tracing is used to treat 2-D aspects of the wave propagation but a 1-D kinetic absorption code is used to determine the local absorption profile within the resonance layer. Both of these two methods are currently under consideration for future upgrades to the simulation package.

Exhaustive comparisons between power deposition profiles obtained with ray tracing versus those obtained from full field methods have not been systematically studied. However, some initial comparisons indicate that in regimes in which mode conversion is not prevalent or in which absorption is strong, so that cavity modes do not dominate the wave fields, that reasonable agreement exists between results from the two methods (HWANG *et al.*, 1985; BRAMBILLA and KRUCKEN, 1988; TIBONE *et al.*, 1988; PHILLIPS *et.a.*,. 1989). The main difference between solutions obtained from the two approaches is that ray tracing tends to predict that the power deposition profiles are more peaked than the full field methods would indicate,though the net power transferred to background ions and electrons tends to agree between the two methods. In the cases in which absorption is weak, results from 2-D full field codes indicate that the formation of global cavity modes can have a strong influence on the wave fields and power deposition profiles (ITOH, ITOH and FUKUYAMA, 1984; SMITHE *et al.*, 1987; BRAMBILLA and KRUCKEN, 1988). The actual structure of the fields in these cases is dependent on the details of the launched $k_{//}$ spectrum, on the actual shape of the vacuum vessel walls, and perhaps on the boundary conditions chosen at the plasma edge and vessel walls. Since these factors are not well-known, the extent to which even the full field methods can accurately model a particular experiment in which absorption is weak is uncertain.

As mentioned previously, the Fokker-Planck model included in RAZE is valid only for particle distribution functions which are isotropic in velocity space. Bounce-averaged Fokker-Planck models have been developed which can treat velocity-space anisotropies but which require significantly more cpu time than the isotropic models. The current WHIST/RAZE package typically uses 20-50 minutes of CRAY-XMP time in simulating ICRF-heated plasmas in such devices as PLT, TFTR, JET, and BPX, where the total elapsed transport time ranges from 0.5 to 10 seconds. The use of bounce-averaged Fokker-Planck models in predictive codes would significantly increase the amount of time required for a simulation. It may be possible, however, to include an enhanced model which addresses some of the effects related to anisotropy by using a modified velocity moments solution of the Fokker-Planck equation (ANDERSON, ERIKSSON, and LISAK, 1985; MORISHITA, FUKUYAMA and FURUTANI, 1988) Such models are currently under consideration.

In summary, the WHIST/RAZE predictive transport simulation package is a flexible and potentially powerful tool to aid in the understanding of ICRF-heated tokamaks. Various transport models can be easily tested with the code against the existing experimental database, with some hope that the heating terms are modeled adequately. Given a transport model which the community feels represents the current experiments and which has a sufficiently sound theoretical basis to be scalable to the next generation of devices, the simulation package can then be used to project a range of performance characteristics that might be expected from such devices.

Acknowledgements - We are grateful for the support and insight given over the course of this project by Drs. J. Hosea, C.F.F. Karney, P. Rutherford, and J.R. Wilson. This research was supported in part by U.S.D.O.E. Contract Nos. DE-AC02-76CHO3073 and DE-AC05-84OR21400.

REFERENCES

ANDERSON, D., ERIKSSON, L.-G., AND LISAK, M. (1985) *Nucl. Fusion* **25**,1751.

ATTENBERGER, S.E., HOULBERG, W.A., and HIRSHMAN, S.P. (1987) *J. Comp. Phys.* **72**,435.

BATCHELOR, D.B., JAEGER, E.F., and COLESTOCK, P.L. (1989) *Phys. Fluids B* **1**, 1174.

BERNSTEIN, I.B. (1975) *Phys. Fluids* **18**,320.

BHATNAGAR, V.P. et al. (1990) *Plasma Phys. Contr. Fusion* **31**,2111.

BITTER, M., et al. (1981) private communication.

BRAMBILLA, M., and KRUCKEN, T. (1988) *Nucl. Fusion* **28**,1813.

CHIU, S.C. (1989) private communication.

CHRISTIANSEN, J.P. et al. (1990) ITER Project Report #ITER-IL-PH-4-1-1 (unpublished).

EDERY, D., PICQ, H., SAMAIN, A., and GAMBIER, D. (1987) *Numerical Modelisation of RF Waves in the Ion Cyclotron Range of Frequency for Tokamak Plasmas* , Rep. EUR-CEA-FC-1334, Association Euratom-CEA, St. Paul lez Durances.

FUKUYAMA, A., ITOH, K., and ITOH, S.-I. (1986) *Comput. Phys. Rep.* **4**,137.

GILL, R.D., et al. (1986) *Proc. of the Thirteenth European Conf. on Controlled Fusion and Plasma Heating, Schliersee, West Germany, 1986*, European Physical Society, Petit-Lancy, Switzerland, Vol. 1, 21.

GOLDSTON, R.J. (1984) *Plasma Phys.* **26**,87.

GOLDSTON, R.J., NEILSON, G.H. et al. (1991) BPX Project Report #X-910311-PPL-22; to be published in *Fusion Technology* (April 1992).

GOLDSTON, R.J., BATEMAN, G. et al. (1991) *18th European Conf. on Controlled Fusion and Plasma Physics*, Berlin, Germany, *Europhysics Conf. Abstracts* Vol. 15C, Part I, I-93.

HAMMETT, G.W., COLESTOCK, P.L. *et al.* (1989), *Proc.* 16th *EPS Conference on Controlled Fusion and Plasma Physics (Venice)*, Vol. **1**,131.

HAMMETT, G.W. (1986) Ph.D. Thesis, Princeton University.

HAWRYLUK, R.J. (1979) *Course on Physics of Plasmas Close to Thermonuclear Conditions, Varenna, Italy* , ed. COPPI, B. *et.al.* , CEC, Brussels, 1980, Vol. **1**,19.

HAWRYLUK, R. J. (1991), "Overview of TFTR Transport Studies", Invited Review Paper, *18th European Conf. on Controlled Fusion and Plasma Physics*, Berlin, Germany, to be published in *Plasma Phys. Contr. Fusion.*

HIRSHMAN, S.P. and WHITSON, J.C. (1983) *Phys. Fluids* **26**,3553.

HOSEA, J.C., PHILLIPS, C.K., et al. (1990), "ICRF Sawtooth Stabilization - Application on TFTR and CIT", to be published in *Theory of Fusion Plasmas (Proc. Joint Varenna-Lausanne Int. Workshop, Varenna, 1990)*, Editrice Compositori, Bologna.

HOULBERG, W.A., ATTENBERGER, S.E., and LAO, L.L (1982) Oak Ridge National Lab. Rep. ORNL/TM-8193; also in *Advances in Mathematical Methods for the Solution of Nuclear Engineering Problems (Proc. ANS/ENS Int. Topical Meeting Munich, 1981)* , Vol. **2**, 425.

HOULBERG, W.A., MILORA, S.L., TOLLIVER. J.S., AND PHILLIPS C.K. (1989) *Pellet Injection and Toroidal Confinement, Proc. of IAEA Technical Committee Meeting, Gut Ising, FRG, October 24-26, 1988*, IAEA Report IAEA-TECDOC-534, 137.

HWANG, D.Q., KARNEY, C.F.F., *et al.* (1983) *Modeling of ICRF Heating of a Tokamak Plasma*, Princeton Plasma Physics Laboratory Report 1990, May 1983 .

HWANG, D.Q., HOSEA, J., *et al.* (1983) *Phys. Rev. Lett.* **51**,1865.

HWANG, D.Q., COLESTOCK, P.L., and PHILLIPS, C.K. (1985) *"The Theory of Minority Species Fast Magnetosonic Wave Heating in a Tokamak"*, in *Wave Heating and Current Drive in Plasmas*, ed. Granatstein, V.L. and Colestock, P.L., Gordon Breach Science Publishers, New York, 1.

ITOH, K., ITOH, S.-I., and FUKUYAMA, A. (1984) *Nucl.. Fusion* **24**,13.

KENNEL, C.F. and ENGELMANN, F. (1966) *Phys. Fluids* **9**,2377.

KERBEL, G.D. and MCCOY, M.G. (1985) *Phys. Fluids* **28**,3629.

KRUCKEN, T. and BRAMBILLA, M. (1989) *Plasma Phys. Contr. Fusion* **31**,157.

LAO, L.L., HIRSHMAN, S.P., and WEILAND, R.M. (1981) *Phys. Fluids* **24**,1431.

MAZZUCATO, E., *et al.* (1985) *Proc. Tenth Int. Conf. on Plasma Phys. and Controlled Nuclear Fusion Research , London*, Vol. **1**, 433.

MORISHITA, T., FUKUYAMA, A. and FURUTANI, J., (1988) *J. Phys. Soc. Jpn.* **57**, 1238.

PARK, W. and MONTICELLO, D.A.,(1990) *Nucl. Fusion* **30,2413.**

PARKER, R., *et al.* (1989) *Proc. of the Twelfth Int. Conf. on Plasma Physics and Controlled Nuclear Fusion Research 1988, Nice,* Vol. **3**, 341.

PFEIFFER, W.W., DAVIDSON, R.H., MILLER, R.L., and WALTZ, R.E. (1980) General Atomic Company Rep. GA A-16178, Dec. 1980.

PHILLIPS, C.K., *et al.* (1989) *Eighth Topical Conference on Radio-Frequency Power in Plasmas, Irvine, CA* , ed. MCWILLIAMS, R., American Institute of Physics, NY, 310.

PHILLIPS, C.K. (1985) *Course and Workshop on Applications of RF Waves to Tokamak Plasmas,* ed. BERNABEI, S., GASPARINO, U., and SINDONI, E., Monotypia Franchi, Italy, Vol. **II**, 455.

REDI, M., TANG, W.M., et al. (1987) *Nucl.Fusion* **27**,2001.

REDI, M. and BATEMAN, G. (1991) *Nucl. Fusion* **31**,547.

SIGMAR, D.J. et al. (1990) to be published in *Proceedings of the Thirteenth International Conference on Plasma Physics and Controlled Fusion Research,Washington,D.C. USA, October 1990*, IAEA, Vienna, Austria, paper

IAEA-CN-53/G-1-1.

SMITHE, D.N., COLESTOCK, P.L., KASHUBA, R.J., KAMMASH, T. (1987) *Nucl. Fusion* **27**,1319.

STIX, T. (1962) *The Theory of Plasma Waves* , McGraw-Hill Book Company Inc., NY.

STIX, T. (1975) *Nucl. Fusion* **15**,737.

SWANSON, D.G., CHO, S., PHILLIPS, C.K., HWANG, D.Q., HOULBERG, W. and HIVELY, L. (1987) *Proceedings of the Eleventh International Conference on Plasma Physics and Controlled Fusion Research, Kyoto, Japan , November 1986*, IAEA, Vienna, Austria, vol. **1**, 653.

TIBONE, F., *et al.* (1988), 15th *European Conference on Controlled Fusion and Plasma Heating, Dubrovnik* , Europhysics Conference Abstracts, EPS, Vol. **1**, 709.

TUBBING, B.J.D., JACQUINOT, J.J., STORK, D., TANGA, A. (1989) Nucl. Fusion **29**, 1953.

WILSON, J.R. and the PLT GROUP (1985) *Radiofrequency Plasma Heating (Sixth Topical Conference, Callaway Gardens, GA,1985), AIP Conf. Proc. #129*, AIP, NY, pg. 28.

YUSHMANOV, P.N. et al. (1990) *Fusion Technol.* **30**,1999.

FIGURE CAPTIONS

Fig.1 Good agreement is found between the experimental measurements of the time evolution of the central electron and ion temperatures during ICRF heating with 2.6 MW in the minority ^{3}He mode on PLT, shown in (a), and the corresponding numerical simulation obtained with the WHIST/RAZE package, shown in (b). (Experimental measurements were obtained from MAZZUCATO et al., 1985.)

Fig. 2 Calculated ICRF power deposition profiles to the bulk ions and electrons are displayed for the simulation given in Fig. 1b. According to Mazzucato et al. (1985), the experimentally deduced central heating rate for electrons was about 1.3-1.5 W/cm^3 for ICRF power levels of about 2.5 MW.

Fig. 3 Same as Fig. 1 but with an ICRF power of 4.3 MW. (Experimental measurements were obtained from WILSON et al., 1985.)

Fig. 4 The electron density profile in the nominal BPX discharge studied here is moderately peaked, with $n_e(0)/\langle n_e \rangle_{vol}$ equal to about 1.3 during the flattop stage.

Fig. 5 The time evolution of the plasma current, toroidal magnetic field and ICRF power for the nominal BPX discharge studied here shows that the field and current ramps are negligible during the ICRF heating pulse.

Fig. 6 The time evolution of both the volume-averaged and central electron and ion temperatures in a nominal BPX discharge, as projected using the WHIST/RAZE package are shown in (a) for an assumed ITER89-P confinement scaling and in (b) for ITER-H confinement scaling.

Fig. 7 The calculated ICRF power split to the ions and electrons is shown in (a) for an assumed ITER89-P scaling, and in (b) for an assumed ITER-H scaling. With the higher temperatures achieved with the ITER-H scaling, direct electron heating becomes more important, leading to a more equal power split.

Fig. 8 The projected fusion gain, Q, for the nominal BPX discharges depicted in Fig. 4-6, is ≥5 in the flattop phase, even with the more pessimistic ITER89-P scaling.

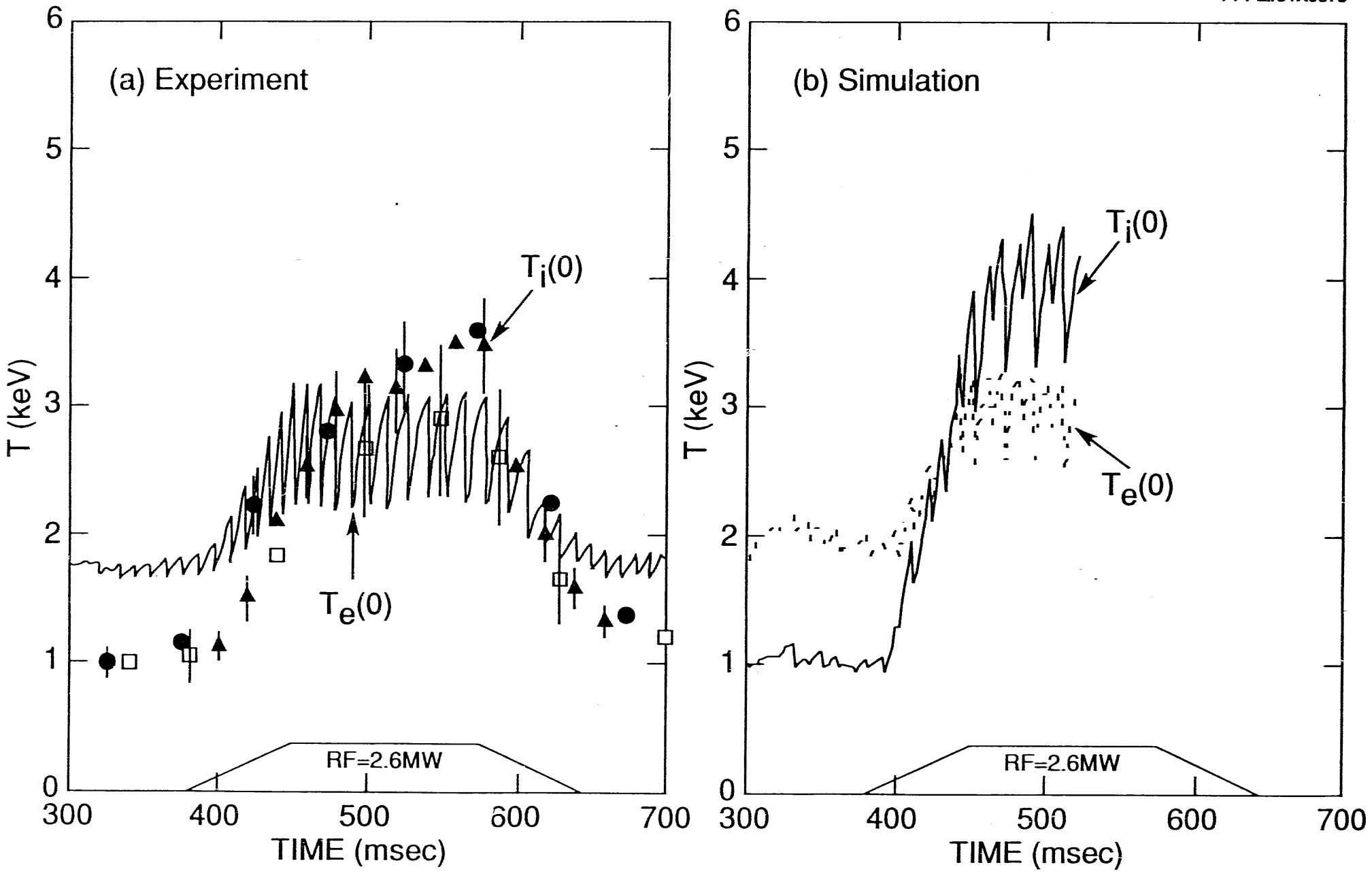
(a) Experiment
(b) Simulation
T (keV)
TIME (msec)
$T_i(0)$
$T_e(0)$
RF=2.6MW
0
1
2
3
4
5
6
300
400
500
600
700

Fig. 1

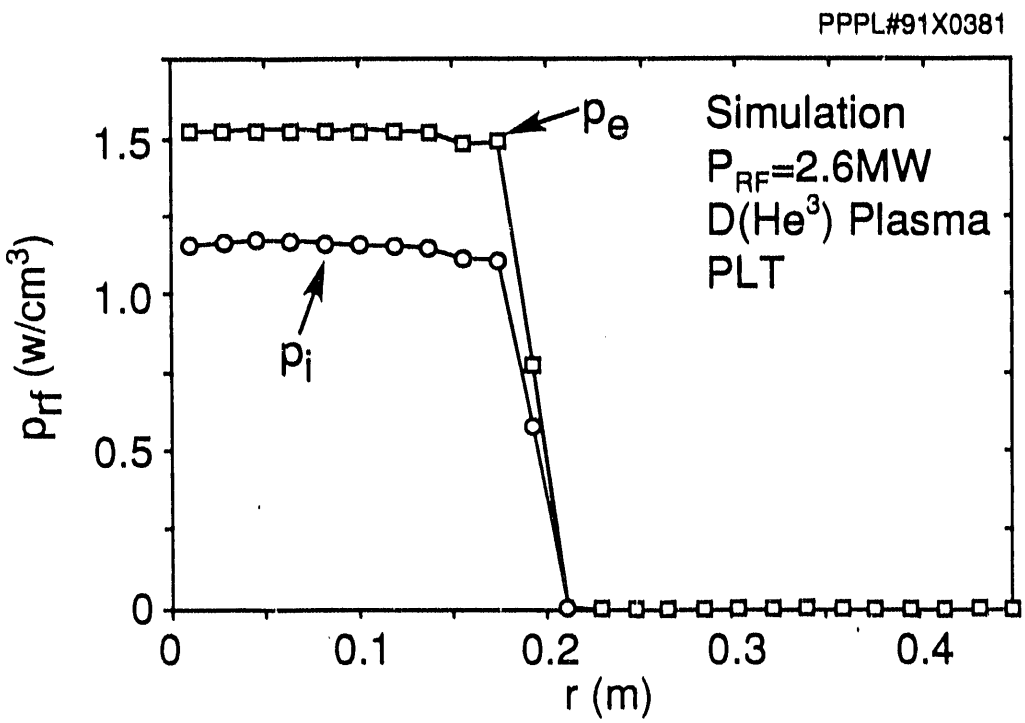
PPPL#91X0381
Simulation
P_{RF}=2.6MW
D(He^3) Plasma
PLT
p_e
p_i
p_{rf} (w/cm^3)
1.5
1.0
0.5
0
0
0.1
0.2
0.3
0.4
r (m)

Fig. 2

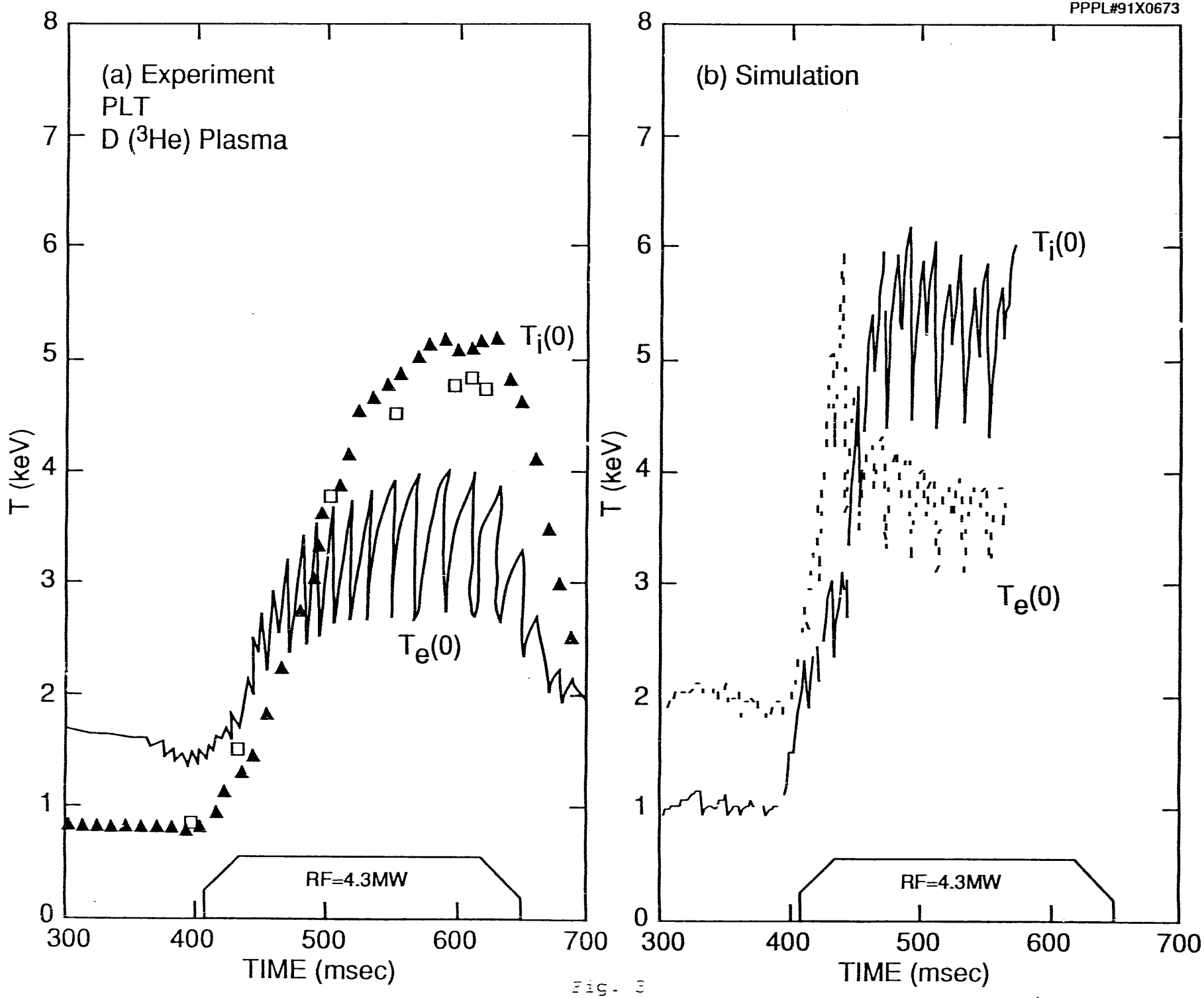
(a) Experiment
PLT
D (^{3}He) Plasma
$T_i(0)$
$T_e(0)$
RF=4.3MW
T (keV)
TIME (msec)
(b) Simulation
$T_i(0)$
$T_e(0)$
RF=4.3MW
T (keV)
TIME (msec)

Fig. 3

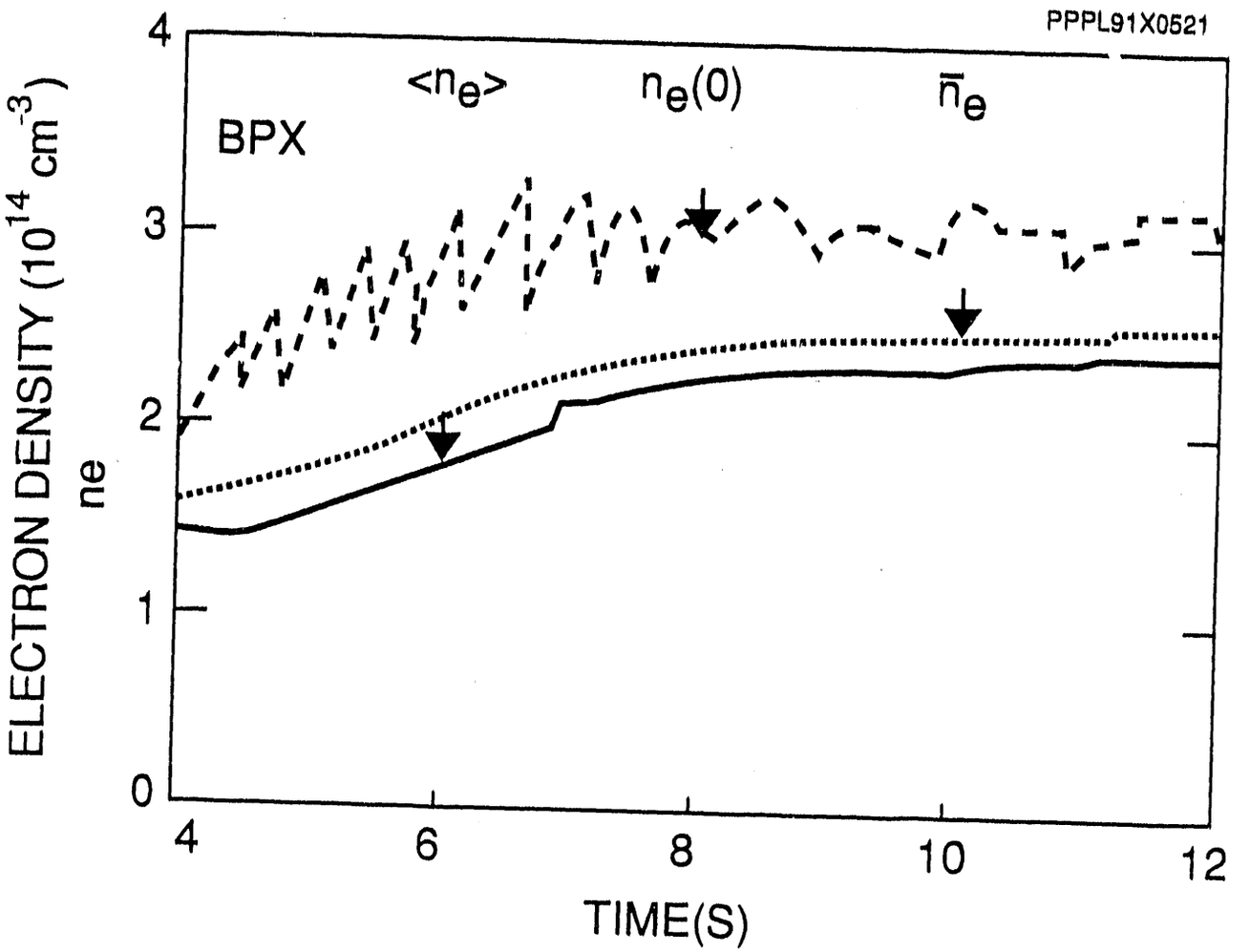
PPPL91X0521
BPX
<ne>
ne(0)
n̄e
ELECTRON DENSITY (10^14 cm^-3)
ne
0
1
2
3
4
4
6
8
10
12
TIME(S)

Fig. 4

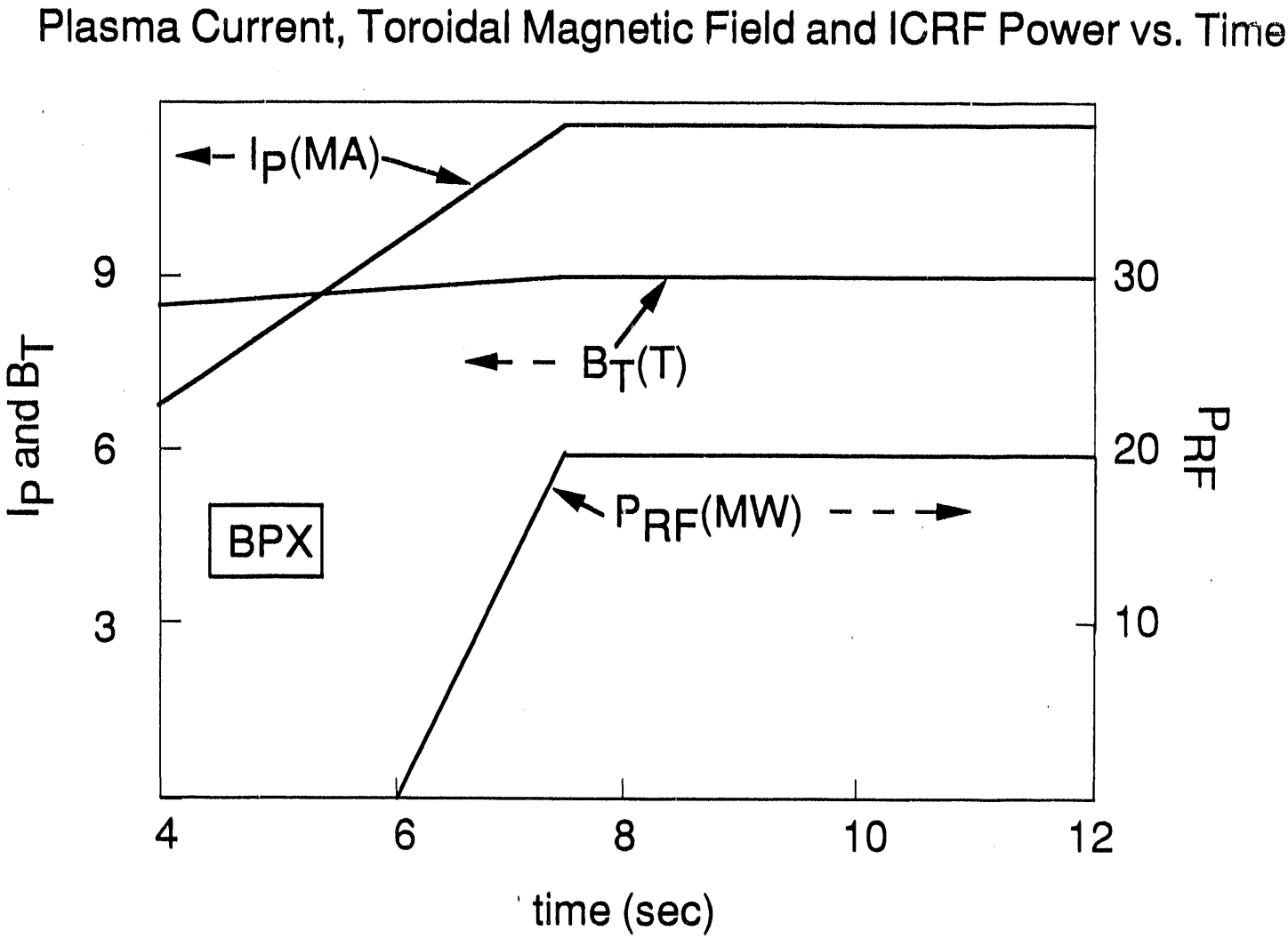
Plasma Current, Toroidal Magnetic Field and ICRF Power vs. Time
Ip(MA)
BT(T)
PRF(MW)
BPX
Ip and BT
PRF
9
6
3
30
20
10
4
6
8
10
12
time (sec)

Fig. 5

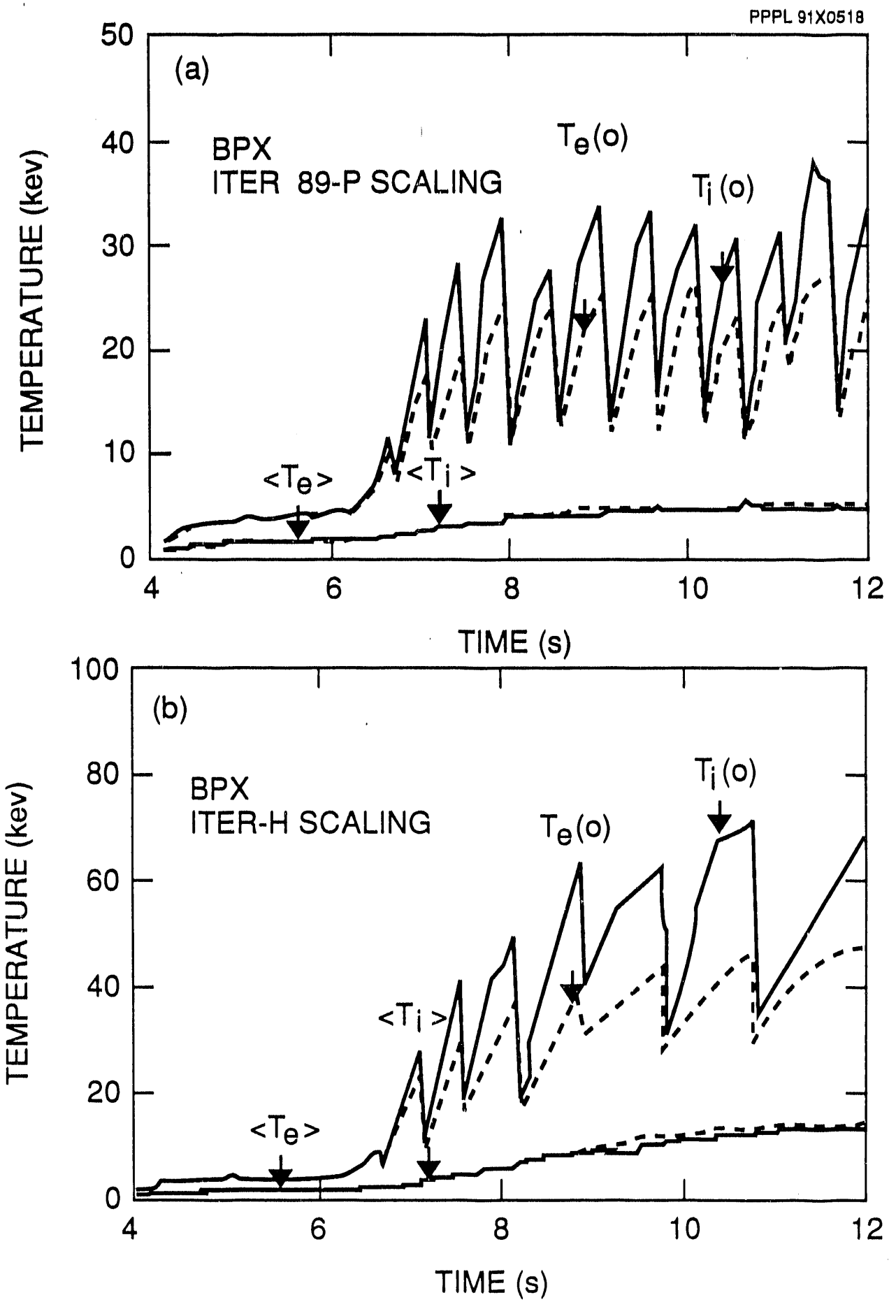
PPPL 91X0518
(a)
BPX
ITER 89-P SCALING
$T_e(o)$
$T_i(o)$
$<T_e>$
$<T_i>$
TEMPERATURE (kev)
TIME (s)
(b)
BPX
ITER-H SCALING
$T_i(o)$
$T_e(o)$
$<T_i>$
$<T_e>$
TEMPERATURE (kev)
TIME (s)

Fig. 6

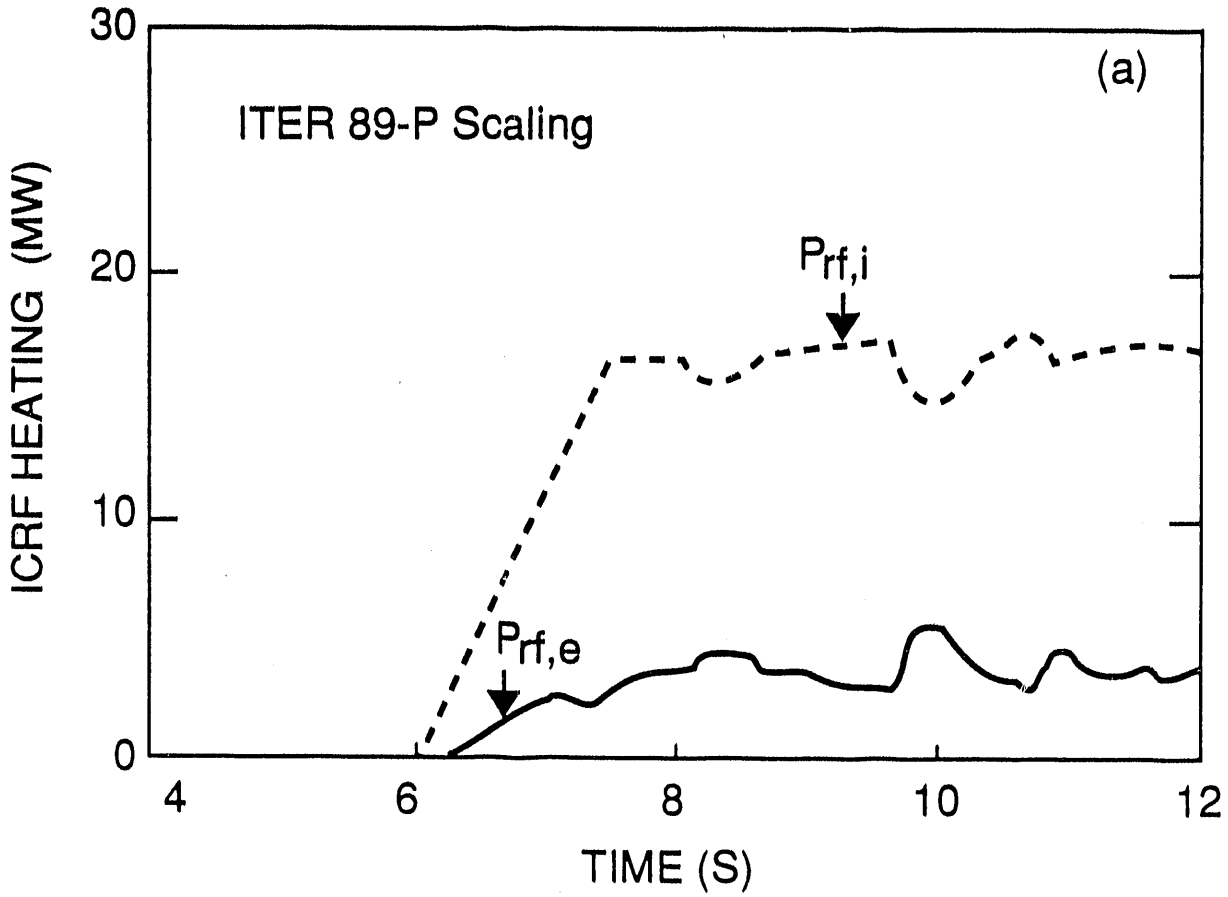
(a)
ITER 89-P Scaling
ICRF HEATING (MW)
30
20
10
0
$P_{rf,i}$
$P_{rf,e}$
4
6
8
10
12
TIME (S)

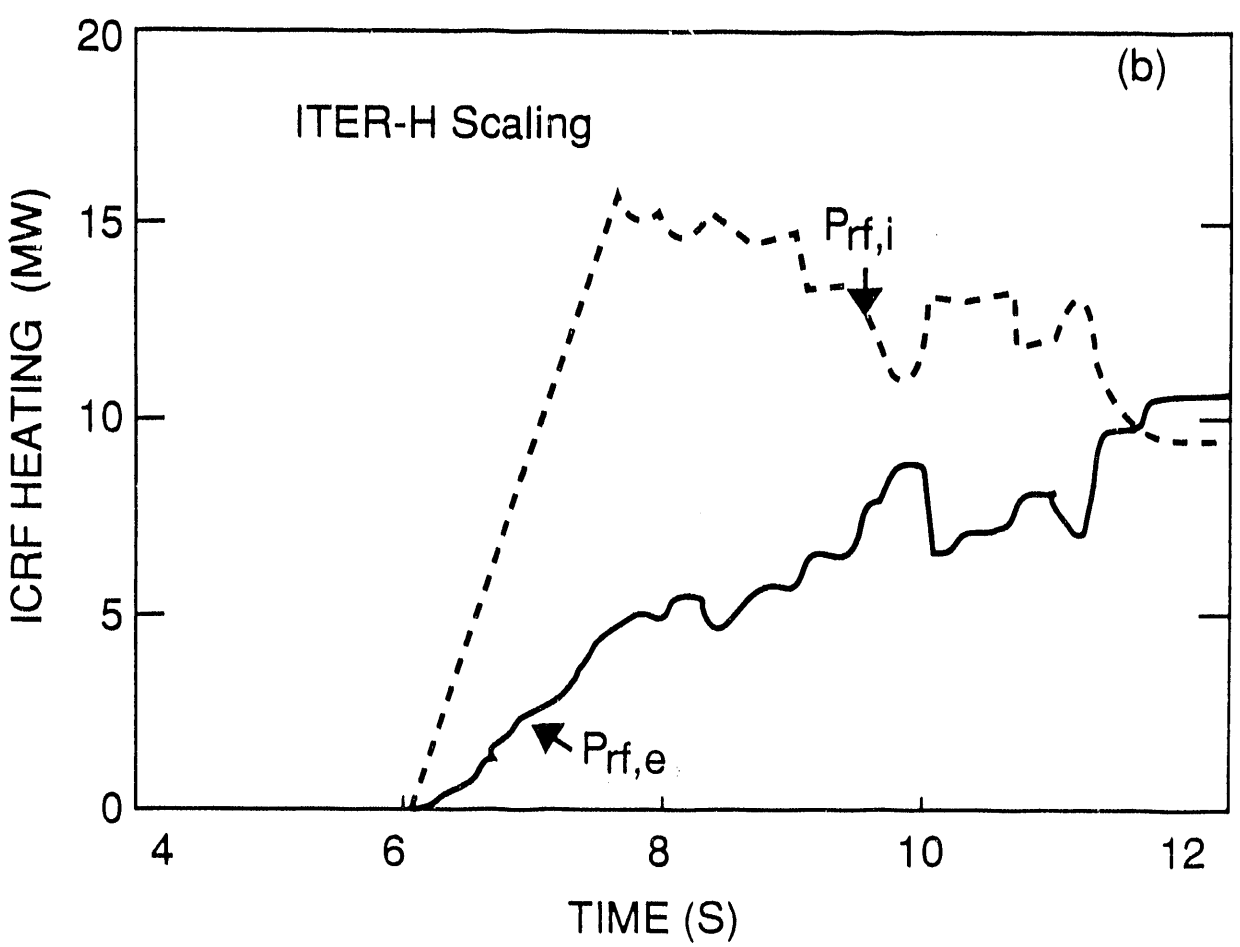
(b)
ITER-H Scaling
ICRF HEATING (MW)
20
15
10
5
0
$P_{rf,i}$
$P_{rf,e}$
4
6
8
10
12
TIME (S)

Fig. 7

PPPL91X0520

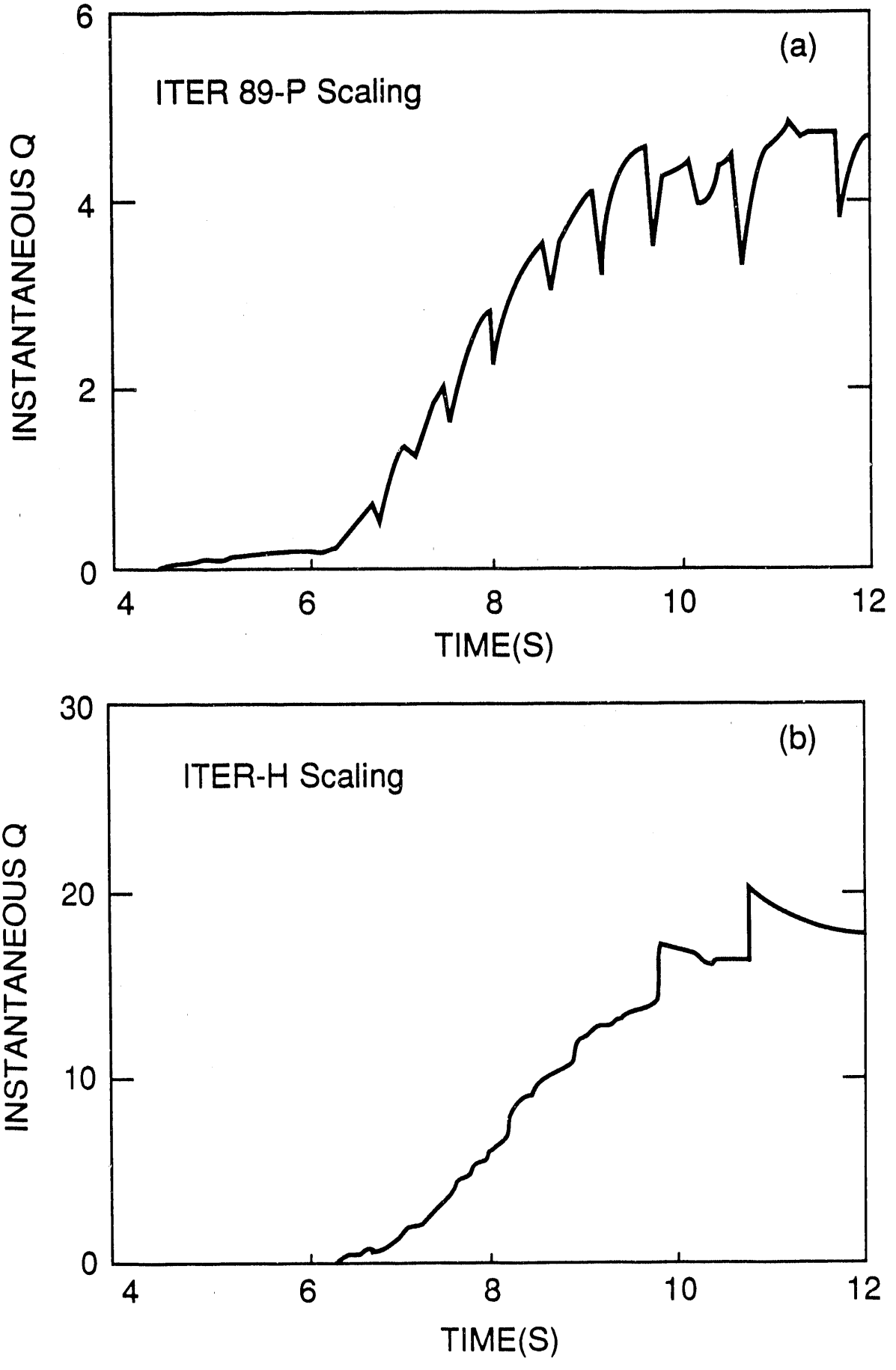

Fig. 8

EXTERNAL DISTRIBUTION IN ADDITION TO UC-420

Dr. F. Paoloni, Univ. of Wollongong, AUSTRALIA
Prof. M.H. Brennan, Univ. of Sydney, AUSTRALIA
Plasma Research Lab., Australian Nat. Univ., AUSTRALIA
Prof. I.R. Jones, Flinders Univ, AUSTRALIA
Prof. F. Cap, Inst. for Theoretical Physics, AUSTRIA
Prof. M. Heindler, Institut für Theoretische Physik, AUSTRIA
Prof. M. Goossens, Astronomisch Instituut, BELGIUM
Ecole Royale Militaire, Lab. de Phy. Plasmas, BELGIUM
Commission-European, DG. XII-Fusion Prog., BELGIUM
Prof. R. Boucique, Rijksuniversiteit Gent, BELGIUM
Dr. P.H. Sakanaka, Instituto Fisica, BRAZIL
Instituto Nacional De Pesquisas Espaciais-INPE, BRAZIL
Documents Office, Atomic Energy of Canada Ltd., CANADA
Dr. M.P. Bachynski, MPB Technologies, Inc., CANADA
Dr. H.M. Skarsgard, Univ. of Saskatchewan, CANADA
Prof. J. Teichmann, Univ. of Montreal, CANADA
Prof. S.R. Sreenivasan, Univ. of Calgary, CANADA
Prof. T.W. Johnston, INRS-Energie, CANADA
Dr. R. Bolton, Centre canadien de fusion magnétique, CANADA
Dr. C.R. James,, Univ. of Alberta, CANADA
Dr. P. Lukác, Komenského Universzita, CZECHO-SLOVAKIA
The Librarian, Culham Laboratory, ENGLAND
Library, R61, Rutherford Appleton Laboratory, ENGLAND
Mrs. S.A. Hutchinson, JET Library, ENGLAND
Dr. S.C. Sharma, Univ. of South Pacific, FIJI ISLANDS
P. Mähönen, Univ. of Helsinki, FINLAND
Prof. M.N. Bussac, Ecole Polytechnique,, FRANCE
C. Mouttet, Lab. de Physique des Milieux Ionisés, FRANCE
J. Radet, CEN/CADARACHE - Bat 506, FRANCE
Prof. E. Economou, Univ. of Crete, GREECE
Ms. C. Rinni, Univ. of Ioannina, GREECE
Dr. T. Mual, Academy Bibliographic Ser., HONG KONG
Preprint Library, Hungarian Academy of Sci., HUNGARY
Dr. B. DasGupta, Saha Inst. of Nuclear Physics, INDIA
Dr. P. Kaw, Inst. for Plasma Research, INDIA
Dr. P. Rosenau, Israel Inst. of Technology, ISRAEL
Librarian, International Center for Theo Physics, ITALY
Miss C. De Palo, Associazione EURATOM-ENEA , ITALY
Dr. G. Grosso, Istituto di Fisica del Plasma, ITALY
Prof. G. Rostangni, Istituto Gas Ionizzati Del Cnr, ITALY
Dr. H. Yamato, Toshiba Res & Devel Center, JAPAN
Prof. I. Kawakami, Hiroshima Univ., JAPAN
Prof. K. Nishikawa, Hiroshima Univ., JAPAN
Director, Japan Atomic Energy Research Inst., JAPAN
Prof. S. Itoh, Kyushu Univ., JAPAN
Research Info. Ctr., National Instit. for Fusion Science, JAPAN
Prof. S. Tanaka, Kyoto Univ., JAPAN
Library, Kyoto Univ., JAPAN
Prof. N. Inoue, Univ. of Tokyo, JAPAN
Secretary, Plasma Section, Electrotechnical Lab., JAPAN
S. Mori, Technical Advisor, JAERI, JAPAN
Dr. O. Mitarai, Kumamoto Inst. of Technology, JAPAN
J. Hyeon-Sook, Korea Atomic Energy Research Inst., KOREA
D.I. Choi, The Korea Adv. Inst. of Sci. & Tech., KOREA
Prof. B.S. Liley, Univ. of Waikato, NEW ZEALAND
Inst of Physics, Chinese Acad Sci PEOPLE'S REP. OF CHINA
Library, Inst. of Plasma Physics, PEOPLE'S REP. OF CHINA
Tsinghua Univ. Library, PEOPLE'S REPUBLIC OF CHINA
Z. Li, S.W. Inst Physics, PEOPLE'S REPUBLIC OF CHINA
Prof. J.A.C. Cabral, Instituto Superior Tecnico, PORTUGAL
Dr. O. Petrus, AL I CUZA Univ., ROMANIA
Dr. J. de Villiers, Fusion Studies, AEC, S. AFRICA
Prof. M.A. Hellberg, Univ. of Natal, S. AFRICA
Prof. D.E. Kim, Pohang Inst. of Sci. & Tech., SO. KOREA
Prof. C.I.E.M.A.T, Fusion Division Library, SPAIN
Dr. L. Stenflo, Univ. of UMEA, SWEDEN
Library, Royal Inst. of Technology, SWEDEN
Prof. H. Wilhelmson, Chalmers Univ. of Tech., SWEDEN
Centre Phys. Des Plasmas, Ecole Polytech, SWITZERLAND
Bibliotheek, Inst. Voor Plasma-Fysica, THE NETHERLANDS
Asst. Prof. Dr. S. Cakir, Middle East Tech. Univ., TURKEY
Dr. V.A. Glukhikh,Sci. Res. Inst. Electrophys.I Apparatus, USSR
Dr. D.D. Ryutov, Siberian Branch of Academy of Sci., USSR
Dr. G.A. Eliseev, I.V. Kurchatov Inst., USSR
Librarian, The Ukr.SSR Academy of Sciences, USSR
Dr. L.M. Kovrizhnykh, Inst. of General Physics, USSR
Kernforschungsanlage GmbH, Zentralbibliothek, W. GERMANY
Bibliothek, Inst. Für Plasmaforschung, W. GERMANY
Prof. K. Schindler, Ruhr-Universität Bochum, W. GERMANY
Dr. F. Wagner, (ASDEX), Max-Planck-Institut, W. GERMANY
Librarian, Max-Planck-Institut, W. GERMANY
Prof. R.K. Janev, Inst. of Physics, YUGOSLAVIA

END

DATE FILMED

4/02/92